Electronic Supplementary Material (ESI) for Inorganic Chemistry Frontiers.

Supporting Information

MnO synergizes with FeC-FeN in carbon nanofiber to boost oxygen reduction for zinc-air batteries

Shuhua Liu[a], Zhiran Sun[a], Yajie Guo[a], Fuxian Zheng[a], Bing Nan[b], Wenjun Kang[a], Konggang Qu[a], Lei Wang[a], Rui Li[a], Zongge Li*[a], Shenglin Xiong*[c] and Haibo Li*[a]

[a] Shandong Provincial Key Laboratory of Chemical Energy Storage and Novel Cell technology, School of Chemistry and Chemical Engineering, Liaocheng University, Liaocheng 252059, China. Email: lizongge@lcu.edu.cn, haiboli@mail.ustc.edu.cn

[b] Shanghai Synchrotron Radiation Facility, Shanghai Advanced Research Institute, Chinese Academy of Sciences, Shanghai 201210, China

[c] Key Laboratory of the Colloid and Interface Chemistry Ministry of Education, School of Chemistry and Chemical Engineering, Shandong University, Jinan 250100, China. Email: chexsl@sdu.edu.cn

Experimental section

Materials

Polyvinylpyrrolidone (PVP) and 4,4-bipyridine ($C_{10}H_8C_2$, 99.68%) were purchased from Shanghai Bidd Pharmaceutical Technology Co., Ltd. N, N-dimethylformamide (DMF, AR) was acquired from Tianjin Kemiou Chemical Reagent Co., Ltd. Ferric chloride hexahydrate ($FeCl_3·6H_2O$, 99%) was procured from Aladdin Company. Manganese acetate tetrahydrate ($Mn(Ac)_2·4H_2O$, 99%) was purchased from Shanghai Sinopharm Chemical Reagent Co., Ltd. Polyacrylonitrile (PAN) was obtained from Sigma-Aldrich. Pt/C (20 wt.%) was purchased from Shanghai Hesen Electric Co., Ltd. All chemicals were used without further purification.

Synthesis of catalysts

Synthesis of Fe_4Mn_4-NC-800

$FeCl_3·6H_2O$ (4 mmol) and $Mn(Ac)_2·4H_2O$ (4 mmol) was dissolved in DMF (5.0 mL). To the resulting solution, 4,4-bipyridine (0.2 mmol, 250 mg) was added and the solution was stirred at room temperature for 2 hours. Then, PVP (250 mg) and PAN (250 mg) were added to the solution, which was magnetically stirred for 20 hours at room temperature. This resulted in the final electrospinning solution.

The electrospinning process was carried out with a direct current voltage of 10.85 kV, 10.0 cm between the syringe and the collector, and a solution supply rate of 8 μL min^{-1}. The fibers produced were air-dried overnight at room temperature. These fibers were pre-oxidized at 280 °C for 1 hour and then heated up to 800 °C for 2 hours under an Ar atmosphere. The heating rate for the entire process was 5 °C min^{-1}. The final product was labeled as Fe_4Mn_4-NC-800.

Synthesis of Fe-NC-800, Mn-NC-800, and NC-800

Only one type of metallic salt, either $FeCl_3·6H_2O$ (4 mmol) or $Mn(Ac)_2·4H_2O$ (4 mmol), was added, while the remaining operation steps were identical to Fe_4Mn_4-NC-800. As a result, the products obtained were identified as Fe-NC-800 and Mn-NC-800,

respectively. For comparison, NC-800 was synthesized without any metal salts.

Synthesis of A-Fe_4Mn_4-NC-800

The Fe_4Mn_4-NC-800 prepared above was placed in 1 M HCl and then stirred rapidly for 10 h. After that, A-Fe_4Mn_4-NC-800 was obtained by centrifugation and washed with deionized water to neutral.

Material characterizations

X-ray diffraction (XRD) analyses were conducted with a Rigaku SmartLab 9 X-ray diffractometer (Cu Kα, λ = 1.5418 Å). X-ray photoelectron spectroscopy (XPS) tests were performed on a Thermo Scientific ESCLAB 250Xi spectrometer. The Raman spectra were examined using a Renishaw InVia Reflex confocal microscope (λ_{ex} = 532 nm). Scanning electron microscope (SEM) analyses were performed on a Thermo Fisher Scientific FIB-SEM GX4. Transmission electron microscopy (TEM) and high-angle annular dark-field transmission electron microscopy (HAADF-STEM) analyses were conducted with a FEI Talos F200x (acceleration voltage: 200 kV). Brunauer-Emmett-Teller (BET) was tested by Micromeritics ASAP 2460 in a nitrogen-saturated atmosphere. The test results were analyzed by Barrett-Joyner-Helenda (BJH) technique to establish the distribution and size of the pores. X-ray absorption fine structure (XAFS) spectra at Fe K-edge were measured at the beamline BL16U1 station of institute of high energy physics (Shanghai, China).

Electrochemical measurement

All electrochemical measurements were performed on a CHI 604E or CHI 760C electrochemical workstation (Shanghai Chenhua Co., Ltd., China) using a standard three-electrode system. The reference electrode used was Ag/AgCl with a saturated KCl solution, while the counter electrode was a Pt wire with a diameter of 0.5 mm and a length of 23 cm. All potentials were converted to reversible hydrogen electrode (RHE) using the Nernst equation: $E_{RHE} = E_{Ag/AgCl}^{\theta} + 0.059pH + E_{Ag/AgCl}$

The oxygen reduction reaction (ORR) test was performed using a 0.10 M KOH

electrolyte, which was saturated with O_2 flux for 30 minutes prior to the experiment. The catalyst ink was prepared as follows: 5 mg catalyst powder was dispersed in a solution consisting of 495 μL ethanol, 495 μL distilled water, and 10 μL Nafion (5 wt.%). The resulting mixture was sonicated for 30 minutes to create a homogeneous catalyst ink. The working electrode was then fabricated by dropping the catalyst ink onto the rotating ring-disk electrodes (RRDE) surface, resulting in a catalyst loading of 0.80 mg/cm^2.

The catalytic activity of ORR was evaluated using cyclic voltammetry (CV) and linear sweep voltammetry (LSV) techniques with respective scan rates of 50 and 10 mV s^{-1}. The electron transfer number (n) was determined from the slope based on the K-L equation:

$$\frac{1}{J} = \frac{1}{J_K} + \frac{1}{J_L} = \frac{1}{J_K} + \frac{1}{B\omega^{1/2}}$$

$$B = 0.62nFC_{O_2}^{*} D_{O_2}^{2/3} \nu^{-1/6}$$

$$J_k = nFkC_{O_2}^{*}$$

where J, J_K, and J_L are the measured current density, kinetic current density, and the diffusion-limiting current density, respectively. ω is the electrode rotating rate, F represents the Faraday constant (F = 96,485 C mol^{-1}), $C_{O_2}^{*}$ is the bulk concentration of O_2 in 0.10 M KOH (1.2×10^{-6} mol cm^{-3}), D_{O_2} is the diffusion coefficient (1.9×10^{-5} cm^2 s^{-1}), ν is the kinematic viscosity of electrolyte (0.01 cm^2 s^{-1}).

The H_2O_2 yield and electron transfer number (n) can be calculated on RRDE using the following equations:

$$H_2O_2(\%) = 200 \times \frac{I_R/N}{I_D + I_R/N}$$

$$n = \frac{4I_D}{I_D + I_R/N}$$

where I_D is the disk current, I_R is the ring current, and N is the current collection efficiency of Pt ring (0.44).

Zn-air battery

For the assembly of the Zn-air battery, a 6.0 M KOH solution served as the electrolyte and a zinc plate acted as the anode. The air cathode was loaded with commercial Pt/C or Fe_4Mn_4-NC-800 (cathode loading of 2 mg cm^{-2}) onto carbon paper. The mold of the zinc-air battery had an effective area of 1 cm^2. The long-term discharge required a current of 10 mA cm^{-2}, whereas variable-current discharge demanded a current of 2, 5, 10, 20 and 30 mA cm^{-2}.

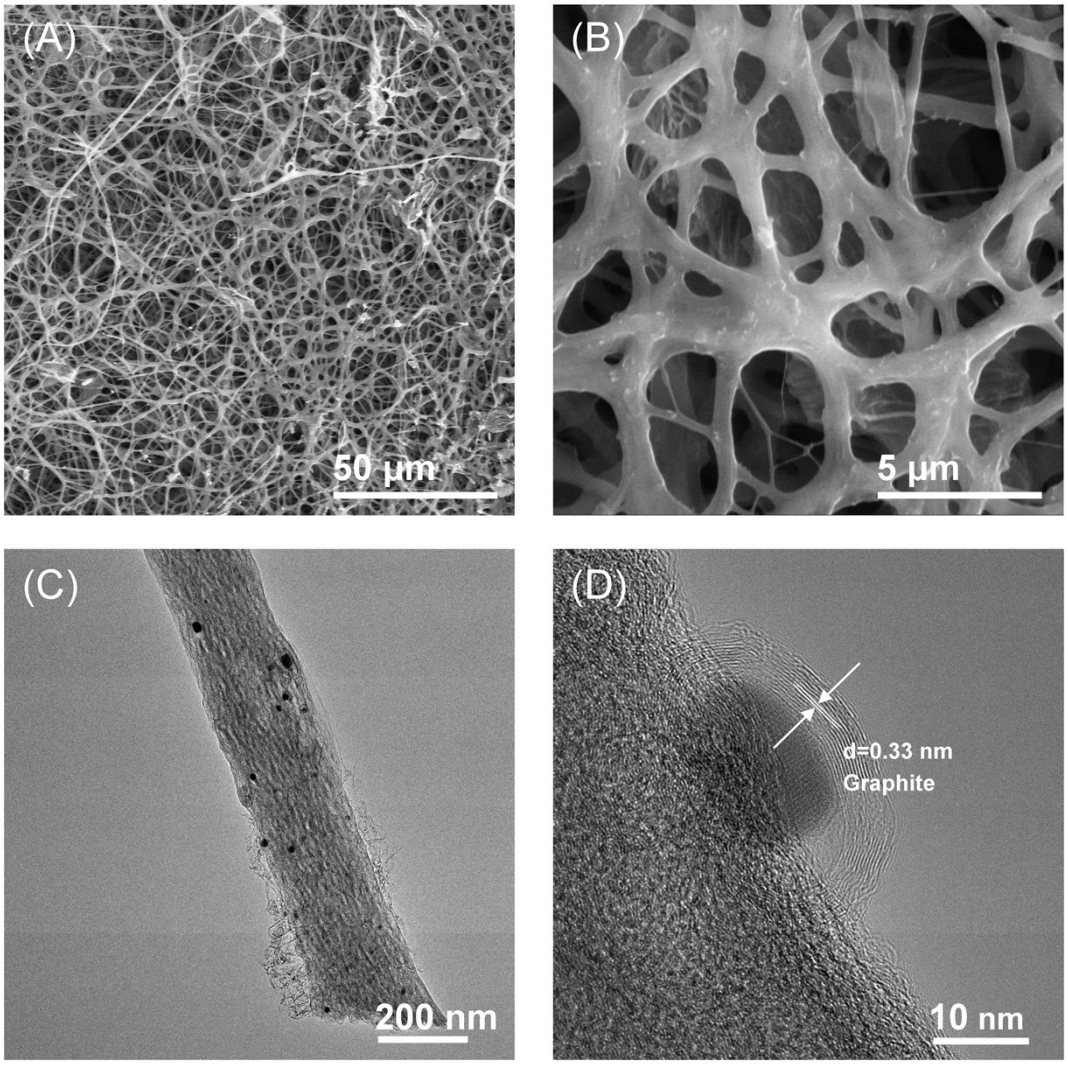

Fig. S1 (A/B) SEM images, (C) TEM image, and (D) HRTEM image of Fe_4Mn_4-NC-800.

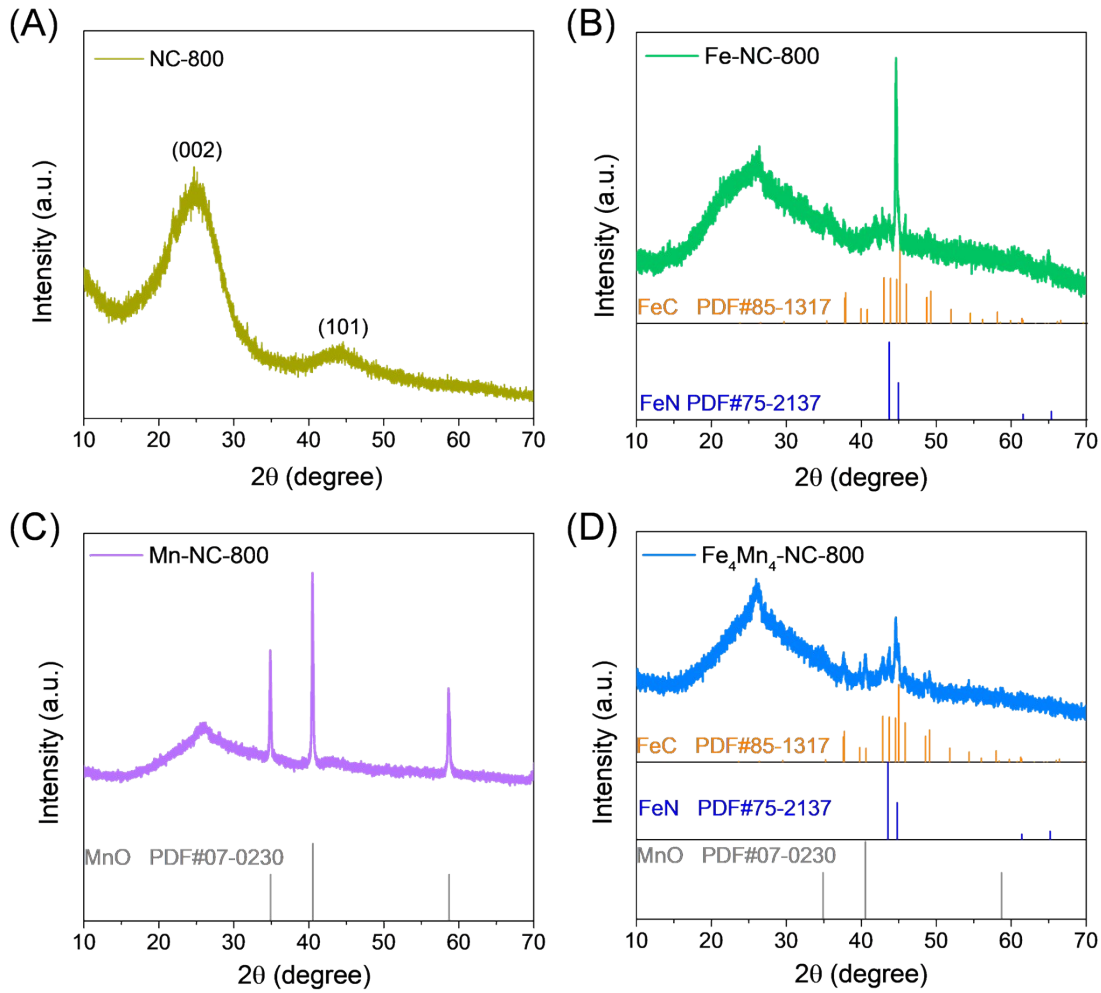

Fig. S2 XRD curves of (A) NC-800, (B) Fe-NC-800, (C) Mn-NC-800 and (D) Fe_4Mn_4-NC-800.

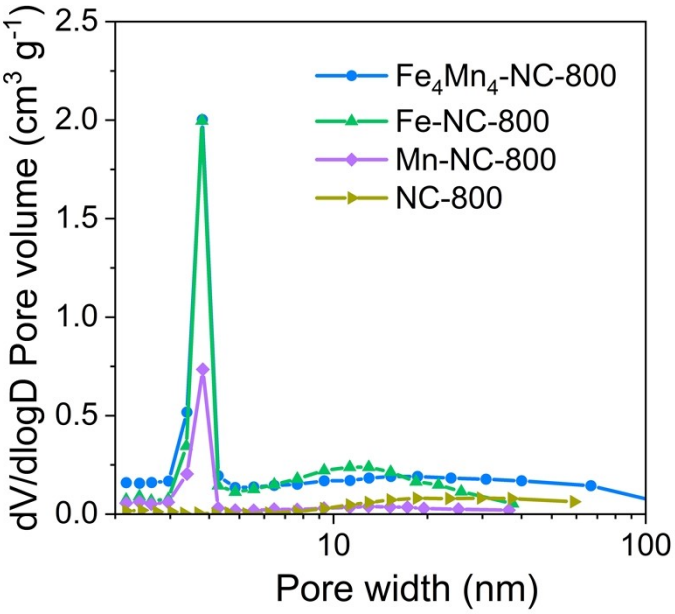

Fig. S3 Pore size distributions of Fe_4Mn_4-NC-800, Mn-NC-800, Fe-NC-800 and NC-800.

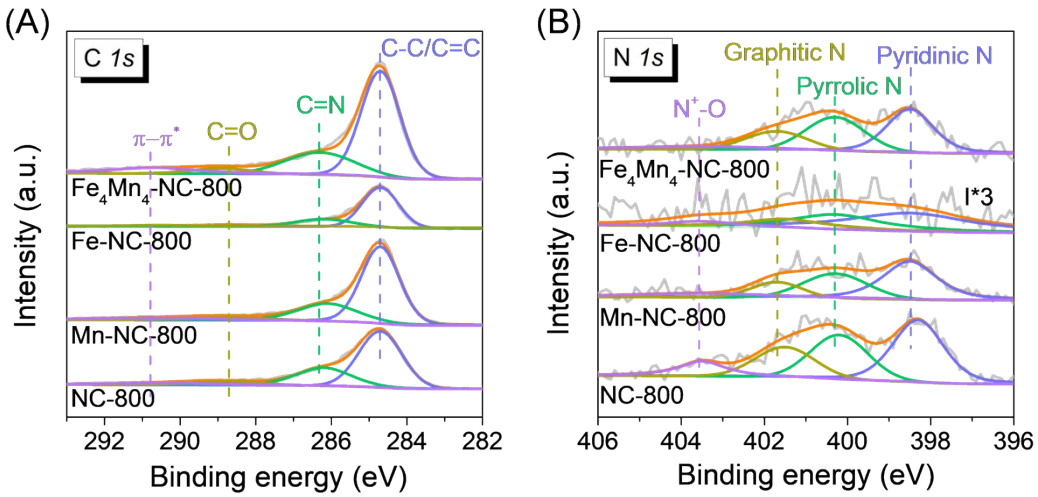

Fig. S4 (A) C 1*s* XPS spectra and (B) N 1*s* XPS spectra of Fe_4Mn_4-NC-800, Fe-NC-800, Mn-NC-800, and NC-800.

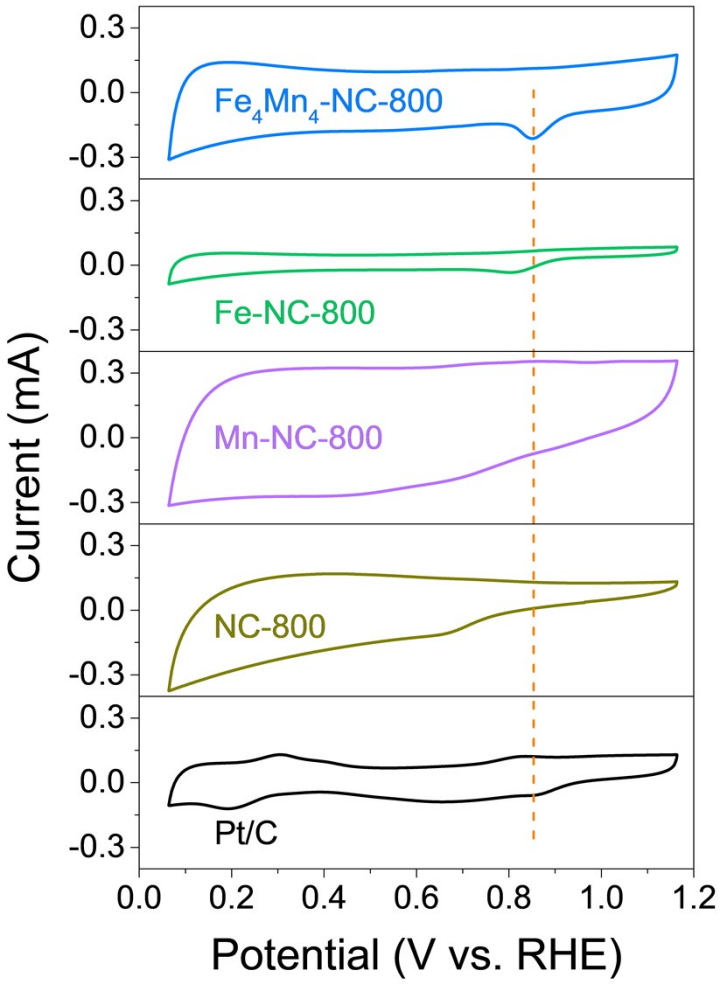

Fig. S5 CV curves at 50 mV s^{-1} in an O_2-saturated 0.1 M KOH.

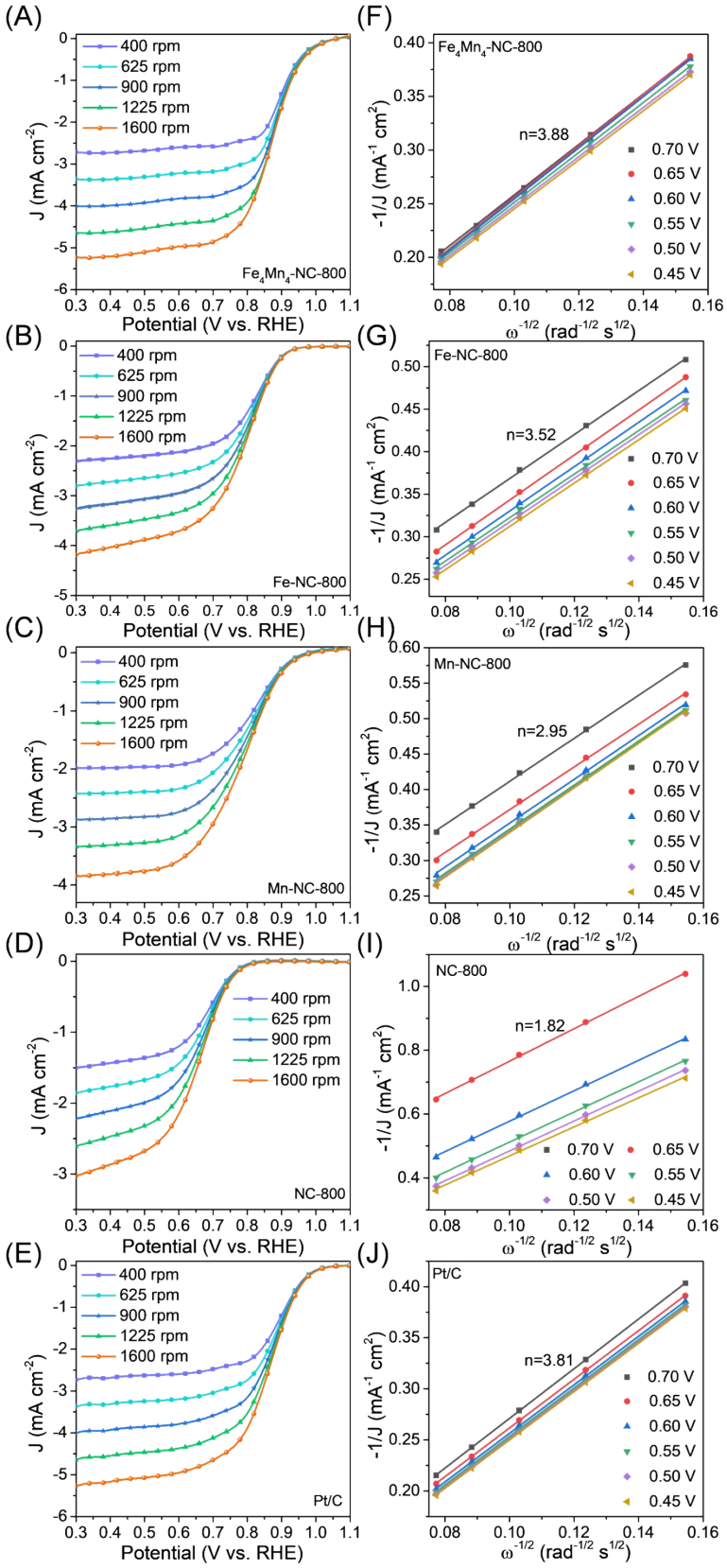

Fig. S6 LSV curves of (A) Fe_4Mn_4-NC-800, (B) Fe-NC-800, (C) Mn-NC-800, (D) NC-800, and (E) Pt/C at different rotation speeds. Corresponding K-L plots of (F) Fe_4Mn_4-NC-800, (G) Fe-NC-800, (H) Mn-NC-800, (I) NC-800, and (J) Pt/C.

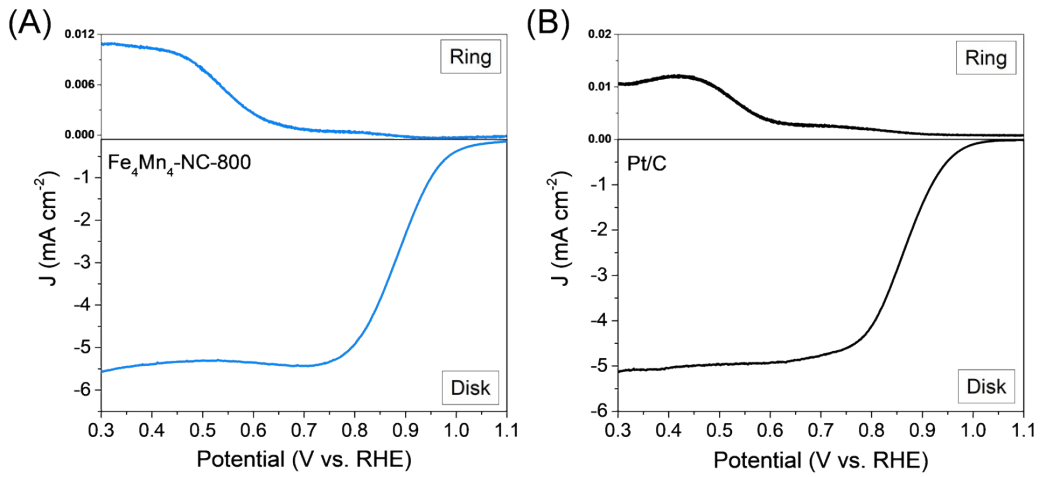

Fig. S7 LSV curves tested on the RRDE for (A) Fe_4Mn_4-NC-800 and (B) commercial Pt/C in an O_2-saturated 0.1 M KOH at 1600 rpm.

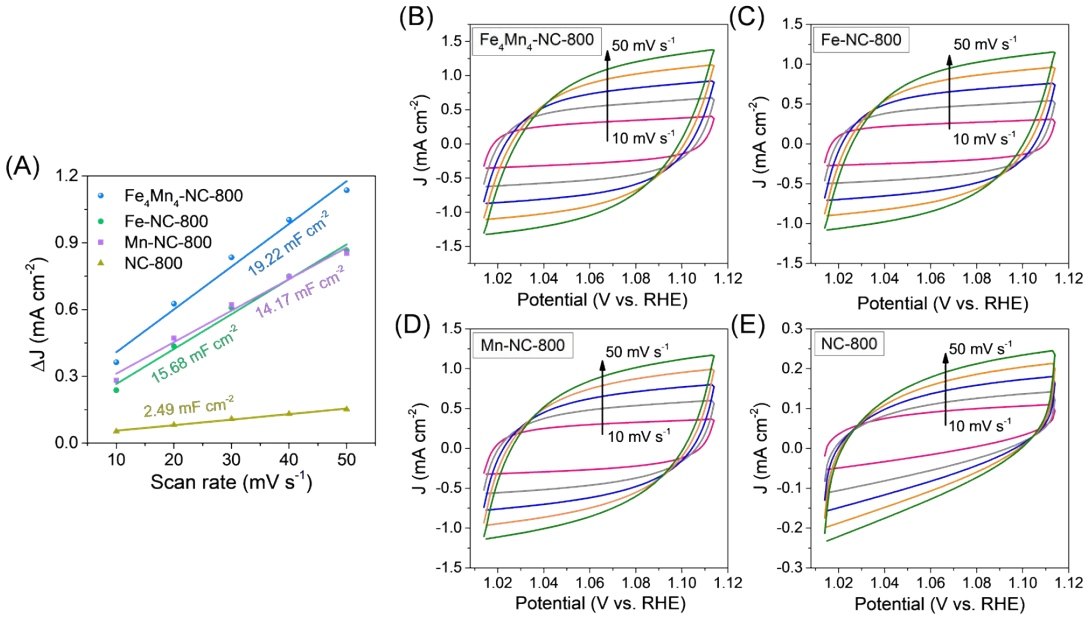

Fig. S8 (A) Plots of current density versus scan rate. CV curves of (B) Fe_4Mn_4-NC-800, (C) Fe-NC-800, (D) Mn-NC-800 and (E) NC-800 at different scan rates in the potential range of 1.015-1.115 V (vs. RHE).

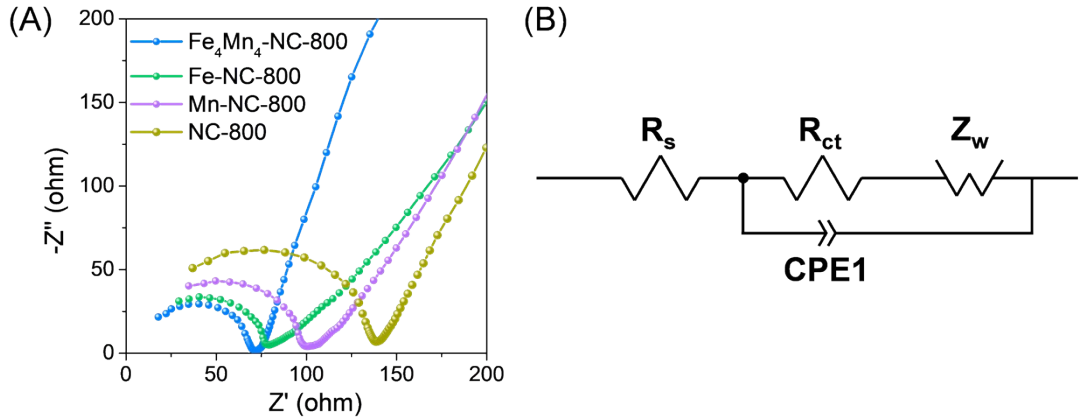

Fig. S9 (A) EIS spectra and (B) Equivalent circuit corresponding to the EIS spectra.

Table S1 The simulated equivalent circuit data of the catalysts.

Catalysts	R_s (Ω cm^{-2})	R_{ct} (Ω cm^{-2})	CPE-T	CPE-P
Fe_4Mn_4-NC-800	8.90	60.7	8.13×10^{-9}	0.9840
Fe-NC-800	6.44	72.6	7.84×10^{-9}	0.9448
Mn-NC-800	3.02	107.4	1.96×10^{-8}	0.8553
NC-800	9.11	128.4	3.52×10^{-9}	0.9765

Table S2 Comparison of ORR performance on various electrocatalysts.

Catalyst	$E_{1/2}$ (V vs. RHE)	E_{onset} (V vs. RHE)	Tafel slop (mV dec^{-1})	Reference
FeCu-DA/NC	0.86	0.96	57	[1]
(Fe,Co)-SA/CS	0.86	0.96	43	[2]
Co/MnO@N,S-CNT/NFs	0.84	0.98	82	[3]
Ni-MnO/rGO	0.78	0.94	85	[4]
CoS/CoO PNRs	0.84	0.95	73.5	[5]
Mn/Co-450	0.78	0.91	90.45	[6]
Co-NiO	0.79	0.92	133	[7]
NiO/CoO TINWs	0.818	0.908	——	[8]
Co-SAs/N–C/rGO	0.84	1.01	67	[9]
CoNC SAC	0.86	0.93	47.9	[10]
MoS_2@Fe-N-C NSs	0.84	0.95	84.7	[11]
Mn/C-NO	0.86	1.0	——	[12]
RGO/ZnPc	0.54	0.82	——	[13]
Fe_3C|Fe–N–C	0.848	0.961	216	[14]
Fe_4Mn_4-NC-800	0.86	1.06	97.06	This Work

References

[1] C. Du, Y. Gao, H. Chen, P. Li, S. Zhu, J. Wang, Q. He and W. Chen, A Cu and Fe dual-atom nanozyme mimicking cytochrome c oxidase to boost the oxygen reduction reaction, *J. Mater. Chem. A*., 2020, **8**, 16994-17001.

[2] V. Jose, H. Hu, E. Edison, W. Manalastas, H. Ren, P. Kidkhunthod, S. Sreejith, A. Jayakumar, J. M. V. Nsanzimana, M. Srinivasan, J. Choi and J. M. Lee, Modulation of single atomic Co and Fe sites on hollow carbon nanospheres as oxygen electrodes for rechargeable Zn–air batteries, *Small Methods.*, 2020, **5**, 2000751.

[3] Q. Zhou, S. Hou, Y. Cheng, R. Sun, W. Shen, R. Tian, J. Yang, H. Pang, L. Xu, K. Huang and Y. Tang, Interfacial engineering Co and MnO within N, S co-doped carbon hierarchical branched superstructures toward high-efficiency electrocatalytic oxygen reduction for robust Zn-air batteries, *Appl. Catal. B: Environ.*, 2021, **295**, 120281.

[4] G. Fu, X. Yan, Y. Chen, L. Xu, D. Sun, J. M. Lee and Y. Tang, Boosting bifunctional oxygen electrocatalysis with 3D graphene aerogel-supported Ni/MnO particles, *Adv Mater.*, 2018, **30**,

1704609.

[5] Y. Wang, X. Wu, X. Jiang, X. Wu, Y. Tang, D. Sun and G. Fu, Citrulline-induced mesoporous CoS/CoO heterojunction nanorods triggering high-efficiency oxygen electrocatalysis in solid-state Zn-air batteries, *Chem. Eng. J.*, 2022, **434**, 134744.

[6] C. Huang, Y. Zhang, X. Li, H. Cao, Y. Guo and C. Zhang, Mn-incorporated Co_3O_4 bifunctional electrocatalysts for zinc-air battery application: An experimental and DFT study, *Appl. Catal. B: Environ.*, 2022, **319**, 121909.

[7] J. Qian, X. Guo, T. Wang, P. Liu, H. Zhang and D. Gao, Bifunctional porous Co-doped NiO nanoflowers electrocatalysts for rechargeable zinc-air batteries, *Appl. Catal. B: Environ.*, 2019, **250**, 71-77.

[8] L. An, B. Huang, Y. Zhang, R. Wang, N. Zhang, T. Dai, P. Xi and C. H. Yan, Interfacial defect engineering for improved portable zinc–air batteries with a broad working temperature, *Angew. Chem. Int. Edit.*, 2019, **58**, 9459-9463.

[9] L. Li, N. Li, J. Xia, S. Zhou, X. Qian, F. Yin, G. He and H. Chen, Metal–organic framework-derived Co single atoms anchored on N-doped hierarchically porous carbon as a pH-universal ORR electrocatalyst for Zn–air batteries, *J. Mater. Chem. A.*, 2023, **11**, 2291-2301.

[10] C.-X. Zhao, J.-N. Liu, J. Wang, C. Wang, X. Guo, X.-Y. Li, X. Chen, L. Song, B.-Q. Li and Q. Zhang, A clicking confinement strategy to fabricate transition metal single-atom sites for bifunctional oxygen electrocatalysis, *Sci. Adv.*, 2022, **8**, 5091.

[11] Y. Yan, S. Liang, X. Wang, M. Zhang, S.-M. Hao, X. Cui, Z. Li and Z. Lin, Robust wrinkled MoS_2 /N-C bifunctional electrocatalysts interfaced with single Fe atoms for wearable zinc-air batteries, *P. Natl A. Sci.*, 2021, **118**, 2110036118.

[12] Y. Yang, K. Mao, S. Gao, H. Huang, G. Xia, Z. Lin, P. Jiang, C. Wang, H. Wang and Q. Chen, O-, N-atoms-coordinated Mn cofactors within a graphene framework as bioinspired oxygen reduction reaction electrocatalysts, *Adv. Mater.*, 2018, **30**, 1801732.

[13] M. Mukherjee, M. Samanta, U. K. Ghorai, S. Murmu, G. P. Das and K. K. Chattopadhyay, One pot solvothermal synthesis of ZnPc nanotube and its composite with RGO: A high performance ORR catalyst in alkaline medium, *Appl.Surf. Sci.*, 2018, **449**, 144-151.

[14] Y. Chen, X. Kong, Y. Wang, H. Ye, J. Gao, Y. Qiu, S. Wang, W. Zhao, Y. Wang, J. Zhou and Q. Yuan, A binary single atom Fe_3C|FeNC catalyst by an atomic fence evaporation strategy

for high performance ORR/OER and flexible Zinc-air battery, *Chem. Eng. J*., 2023, **454**, 140512.